


## Research Article

# Teaching Mode of Japanese Intensive Reading in Colleges and Universities Based on Cloud Computing Intelligent Platform

Xiaohuan Yu <sup>1,2,3</sup> and Zhou Huang<sup>3</sup>

<sup>1</sup>College of Foreign Languages, North China Institute of Science and Technology, Langfang 065201, China

<sup>2</sup>College of Foreign Languages, Xi'an Jiaotong University, Xi'an 710049, China

<sup>3</sup>School of Oriental Languages, Anhui International Studies University, Hefei 231201, China

Correspondence should be addressed to Xiaohuan Yu; 200600739yxh@ncist.edu.cn

Received 11 April 2022; Accepted 16 May 2022; Published 15 June 2022

Academic Editor: Chia-Huei Wu

Copyright © 2022 Xiaohuan Yu and Zhou Huang. This is an open access article distributed under the Creative Commons Attribution License, which permits unrestricted use, distribution, and reproduction in any medium, provided the original work is properly cited.

In order to improve the effect of Japanese teaching in colleges and universities, this study uses the variance of the bias error of the data channel of the cloud transmission platform to represent the intensity of the bias error between the data channels of the cloud transmission platform. Moreover, this study uses the perfect reconstruction filter algorithm to compensate for the frequency-dependent mismatch error of the broadband signal, obtains the value at the ideal sampling point from the sampling sequence estimation, and then corrects the delay deviation. In addition, this study constructs the overall structure of the Japanese intensive reading teaching system in colleges and universities based on the network cloud platform, proposes a method for solving the correction filter, and conducts simulation verification. Finally, this study constructs a teaching system for Japanese intensive reading in colleges and universities based on the network cloud platform. Through experimental research, it is verified that the teaching mode of Japanese intensive reading in colleges and universities based on the cloud computing intelligent platform has certain feasibility.

## 1. Introduction

In traditional Japanese intensive reading teaching in colleges and universities, the teaching of basic knowledge such as vocabulary and grammar has become the center. Although the goal is also to cultivate students' comprehensive abilities in listening, speaking, reading, and writing, the content of the course places great emphasis on grammar teaching and ignores the actual workability of students and the professional quality requirements of specific industries. Therefore, how to enable students to master the Japanese language knowledge and at the same time have the Japanese ability to use Japanese for effective communication in the work environment to complete tasks is a problem that needs to be urgently solved. The ability-based action-oriented teaching model meets this requirement. Therefore, it is particularly necessary to introduce an action-oriented teaching model in the teaching of Japanese intensive reading in colleges and

universities. In addition, how to introduce the action-oriented teaching model into the teaching of Japanese intensive reading class is worthy of our in-depth discussion.

The syllabus for Japanese majors in colleges and universities clearly points out that the goal of the Japanese intensive reading course is to cultivate students with a good foundation in Japanese listening, speaking, reading, writing, translation, etc., and a strong comprehensive ability to use Japanese. Contents such as extensive reading, listening, writing and translation, etc., enable students to truly master relevant knowledge and be able to integrate and flexibly use them, so as to achieve the purpose of truly mastering Japanese. This is completely consistent with the general requirements of the new JLPT. The purpose of teaching is not just for examinations, but examinations are an effective means of testing teaching. After all, the JLPT tests the comprehensive ability to use Japanese, and its performance is an important indicator for students to find jobs and study

abroad. Therefore, it is particularly necessary to explore the teaching mode of Japanese intensive reading courses based on the focus of the reform of the new Japanese language proficiency test, especially to improve students' reading and listening skills.

In order to improve the teaching effect of Japanese intensive reading in colleges and universities, this study combines the network cloud platform to improve the teaching of Japanese intensive reading in colleges and universities, and builds an intelligent Japanese intensive reading teaching system to provide a platform for the subsequent improvement of the quality of Japanese intensive reading teaching.

## 2. Related Work

Through screening and reviewing the sources of literature authors, it is found that cloud computing applied to school management and learning aids has been used as an important research project in many universities. "The American State University has introduced cloud computing-assisted mail to ensure the security of students' e-mail, and other research and development of cloud computing-assisted learning are also underway, for example, the Collaborative Learning Center of Minnesota State University in the United States" [1]. Regarding the research on cloud computing in the storage of teaching resources, the literature [2] proposes the development of cloud storage network teaching resources that can be extracted on demand and supports the establishment of cloud teaching management systems in colleges and universities. Regarding the research on the application of cloud computing to the teaching system of colleges and universities, literature [3] proposes that due to low cost and strong service, cloud computing will replace the existing teaching software service system, and it is necessary to strengthen the cloud computing of the teaching system in colleges and universities.

The design of the cloud classroom platform based on the e-school bag should be based on the overall needs and functional requirements [4]. The system structure of the cloud classroom platform including the education cloud IaaS layer, cloud classroom PaaS layer, cloud classroom SaaS layer and user access terminals, and college cloud classrooms need to be built based on network classrooms, e-book bags, and iPad cloud classrooms [5], and cloud classroom platform design should enrich and promote diverse learning methods, for example, the subversion of teaching mode, the transformation of the learning process, and the use of blended learning methods [5].

The cloud classroom teaching mode includes teacher modules: study guide, classroom exercises, and homework; student module: group construction and discussion stage, modification and application of study guide plans, student demonstration and research stage [6], and cloud classroom interactive visualization layer structure. The design is mainly divided into four layers, namely, the data source layer, data storage layer, data analysis layer, and

data visualization layer [7]. Teachers and students can realize interactive teaching by logging in to the cloud classroom [8]. Cloud classroom teaching is easy to create. The teaching situation is easy to stimulate students' interest in learning, and it is easy to use a variety of teaching methods. Cloud classroom teaching is highly interactive, which is convenient for the course and teacher-student information management. Based on the Baihui cloud computing platform, cloud classroom teaching based on collaborative learning is designed [9].

In recent years, more and more research studies on cloud courses have been conducted. These studies mainly include the following aspects: cloud course connotation, implementation, evaluation, and cloud course teaching. Among them, there are many studies on the connotation and characteristics of cloud courses, and most scholars have reached a consensus on cloud courses as a new course form [10]; there are few studies on the implementation and evaluation of cloud courses, but there are existing studies on cloud courses implementation dilemma and strategy analysis, and the diverse and dynamic evaluation forms are deeply inspiring and provide an important reference for scholars in the future. The research on cloud course teaching mainly includes personalized learning, which highlights the subjectivity and differences of students. Cloud courses are shared and expand teaching information and promote educational equity, etc. [11]. These studies are invaluable and have made certain contributions to the theoretical study of cloud curriculum issues. The deficiencies of the research are as follows: first, since the cloud course is a new course form, its structure, function, and development are very important, and more scholars need to conduct in-depth research in these aspects [12]. Second, the research on the teaching of cloud courses is relatively fragmented, and there is a lack of overall research on the teaching mechanism of cloud courses [13].

The application of cloud computing in teaching has just started. Scholars generally pay more attention to research in this area. They have studied cloud computing in college management, teaching resource storage, and as a school teaching method [14]. Literature [15] explores and analyzes cloud computing as a method to achieve simplified computing, and the research involves many aspects: cloud classroom learning objectives, methods, attitudes, and significance; development and design of cloud classroom platform serving teaching; cloud classroom teaching goals, design, resource management, method selection, implementation process, and teaching evaluation; research on cloud classroom teaching based on specific disciplines; advantages and disadvantages of cloud classroom teaching and offline classroom teaching, etc. [16]. On the whole, the research on cloud classroom teaching is relatively comprehensive and mature. However, there is very little research on the relationship between cloud classroom teaching and offline classroom teaching, and the only research only stays in the comparison of advantages and disadvantages, and the lack of theoretical research is obviously not enough to match its actual importance [17].

### 3. Cloud Computing High-Speed Data Transmission

Under ideal conditions, the sum of input  $x(t)$  and output  $y[n]$  of TI-ADC meets:  $y[n] = x(nT_s)$ , and  $T_s$  is the sampling period of TI-ADC. However, in actual conditions, factors such as front-end conditioning circuits, ambient temperature, differences between ADC chips, and mismatches in design will make the paths not completely consistent. This will cause problems such as mismatch between data channels of the cloud transmission platform, which will cause errors in the output data.

When there is an offset error in the data channel of the cloud transmission platform, the decomposition filter in the HFB model is shown in Figure 1.

$o_m$  is the offset mismatch error of the data channel of the  $m$ -th cloud transmission platform. From the figure, we can get the following:

$$x_m[n] = x[n + m] + o_m. \quad (1)$$

Furthermore, according to the HFB model, the output of TI-ADC can be obtained as follows:

$$Y(e^{j\omega T_s}) = X(e^{j\omega T_s}) + \frac{2\pi}{M} \sum_{m=0}^{M-1} o_m \sum_{k=0}^{M-1} \delta\left(\omega T_s - \frac{2\pi k}{M}\right) e^{-j(2\pi k/M)m}. \quad (2)$$

It can be seen that in addition to the signal component of the output spectrum of the TI-ADC, there are still  $M$  mismatched harmonic components at  $2\pi k/M$ ,  $k = 0, 1, \dots, M-1$ . Moreover, the spurious component has nothing to do with the frequency of the sampled signal. It is only related to the magnitude of the offset error and the number of data channels on the TI-ADC cloud transmission platform.

When the bias mismatches of all paths are the same, that is, when  $o_m = o$ , equation (2) can be simplified to the following:

$$Y(e^{j\omega T_s}) = X(e^{j\omega T_s}) + 2\pi\delta(\omega T_s). \quad (3)$$

This is consistent with the output of a single ADC when there is a bias mismatch. Therefore, we can know that when performing offset error correction on the TI-ADC system, it is not necessary to correct all the offset errors of the data channels of each cloud transmission platform to 0. It is only necessary to ensure that the offset error of each cloud transmission platform data channel is consistent.

We assume that the input sine signal  $x(t) = \sin(2\pi f_c t)$  and the angular frequency is  $\omega_c$ ; then, the power of the signal is as follows:

$$P_s = |X(j\omega)|^2 = \frac{1}{2}. \quad (4)$$

We use the variance of the cloud transmission platform data channel offset error  $\sigma_o^2$  to characterize the strength of the offset error between the cloud transmission platform data channels, and then, the power of the mismatched harmonics can be obtained, as shown below as follows:

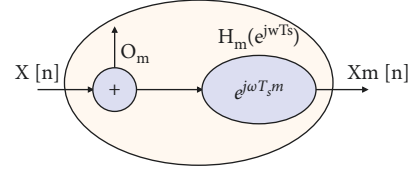


FIGURE 1: Bias mismatch HFB model.

$$P_{\text{offset}} = \frac{1}{M} \sum_{m=0}^{M-1} |o_m|^2 = \sigma_o^2. \quad (5)$$

If the ADC's input full scale is FSR and the number of quantization bits is  $R$ , the quantization noise power of the ADC can be obtained from the literature as follows:

$$N_q = \left( \frac{\text{FSR}}{2^R \sqrt{12}} \right)^2. \quad (6)$$

Therefore, the available SNDR of the TI-ADC system is as follows:

$$\begin{aligned} \text{SNDR}_{\text{offset}} &= 10 \log_{10} \frac{P_s}{P_{\text{offset}} + N_q} \\ &= 10 \log_{10} \frac{1}{2\sigma_o^2 + 2N_q}. \end{aligned} \quad (7)$$

The simulation verification is performed below, and the simulation parameters are set as follows:

- (1) The number of data channels  $N$  of TI-ADC cloud transmission platform is 4.
- (2) The sampling frequency of TI-ADC is  $\omega_s$ .
- (3) The number of quantization bits is 12 bit.
- (4) The frequency of the input sine signal is  $0.1001 \omega_s$ .
- (5) The offset error of the data channel of each cloud transmission platform is Offset = [0.1, -0.1, 0.05, 0.2], and there is no other error.

It can be seen from Figure 2, in addition to the input signal component  $0.1 \omega_s$  and its image component  $0.9 \omega_s$ , that there are also spurious components caused by offset mismatch at  $0, 0.25 \omega_s, 0.5 \omega_s$ , and  $0.75 \omega_s$ . It can be seen that the location of mismatched harmonics has nothing to do with the input signal but only with the number of data channels on the cloud transmission platform. Due to the influence of mismatch spurious components, the system SFDR is only 16.24 dB, SNDR is 16.34 dB, and ENOB is 2.42 bit.

For a single ADC, its own gain error mismatch, that is, the front-end conditioning circuit or internal amplifier, and other analog devices amplify and attenuate the error caused by the different degrees of analog signal amplification. The gain mismatch error in the TI-ADC system is caused by the inconsistent gain coefficients of the data channels of each cloud transmission platform. The HFB model is used to analyze the gain mismatch error.

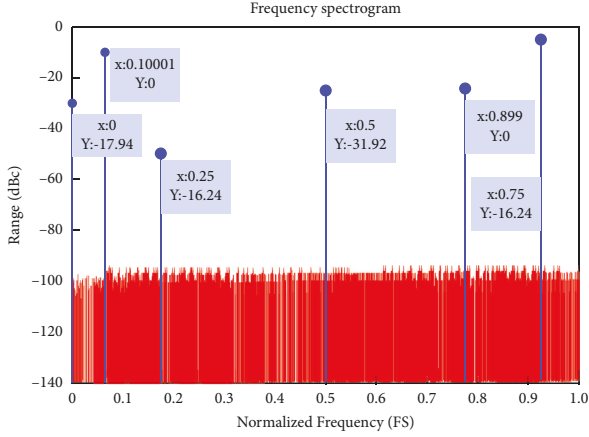


FIGURE 2: Spectral diagram of offset mismatch.

When there is a gain error, the model of the decomposition filter is shown in Figure 3.

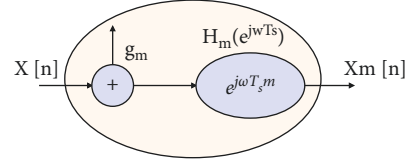


FIGURE 3: Gain mismatch HFB model.

$g_m$  represents the gain error value of the  $m$ -th cloud transmission platform data channel, which is equivalent to multiplying the original signal by a coefficient before sampling and then performing subsequent operations. Therefore, we can get [18] the following:

$$x_m[n] = g_m x[n + m]. \quad (8)$$

Then, substituting it into  $Y(e^{j\omega T_s}) = \sum_{m=0}^{M-1} Y_m(e^{j\omega T_s}) = \frac{1}{M} \sum_{m=0}^{M-1} \sum_{k=0}^{M-1} X(e^{j(\omega T_s - 2\pi k/M)}) H_m(e^{j(\omega T_s - 2\pi k/M)}) G_m(e^{j\omega T_s})$ , we can get the following:

$$Y(e^{j\omega T_s}) = \frac{1}{M} \sum_{m=0}^{M-1} \sum_{k=0}^{M-1} g_m X(e^{j(\omega T_s - 2\pi k/M)}) H_m(e^{j(\omega T_s - 2\pi k/M)}) G_m(e^{j\omega T_s}), \quad (9)$$

$$Y(e^{j\omega T_s}) = \frac{1}{M} \sum_{k=0}^{M-1} \sum_{m=0}^{M-1} g_m e^{-j2\pi km/M} X(e^{j(\omega T_s - 2\pi k/M)}).$$

Analyzing the above equation, it can be seen that in addition to the spectrum components of the original signal, the spectrum of the output signal also contains  $M-1$  mismatched harmonic components. They are located at  $\omega_c + k/M\omega_s$ , and due to the existence of the image component, the mismatched harmonic components in the  $[0, 2\pi)$  range are located at  $\omega_c \pm k/M\omega_s$ .

Further analysis shows that when the gains of the data channels of all cloud transmission platforms are the same, that is, when  $g_m = g$ , the above equation can be simplified to as follows:

$$Y(e^{j\omega T_s}) = gX(e^{j\omega T_s}). \quad (10)$$

This shows that even if there are errors in the data channels of each cloud transmission platform, as long as the error values are consistent, the spectrum can be free of mismatched harmonic components. It can be corrected only by changing the amplitude of the signal component.

In order to facilitate the calculation of the effect of the gain mismatch on the system, we assume that the input signal is  $x(t) = \sin(2\pi f_c t)$ , the angular frequency is  $\omega_c$ , and its Fourier transform is [19] as follows:

$$X(j\omega) = j\pi(\delta(\omega + \omega_c) - \delta(\omega - \omega_c)). \quad (11)$$

Substituting it to formula (10), we can get the following:

$$Y(e^{j\omega T_s}) = \frac{1}{M} \sum_{k=0}^{M-1} \sum_{m=0}^{M-1} g_m e^{-j2\pi km/M} j\pi \left( \delta\left(\omega T_s + \omega_c T_s - \frac{2\pi k}{M}\right) - \delta\left(\omega T_s - \omega_c T_s - \frac{2\pi k}{M}\right) \right). \quad (12)$$

The total signal power in the range of  $[0, 2\pi)$  is as follows:

$$P_s = \frac{1}{2} E[g_m]^2. \quad (13)$$

The gain mismatch harmonic power is as follows:

$$P_{\text{gain}} = \frac{1}{2M} \sum_{m=0}^{M-1} |g_m|^2 - P_s = \frac{1}{2} \sigma_g^2. \quad (14)$$

The variance of the gain mismatch error is  $\sigma_g^2$ . Therefore, when there is a gain mismatch error, the SNDR of the system is

$$\begin{aligned} \text{SNDR}_{\text{gain}} &= 10 \log_{10} \frac{P_s}{P_{\text{gain}} + N_q} \\ &= \frac{E[g_m]^2}{\sigma_g^2 + 2N_q}. \end{aligned} \quad (15)$$

The simulation verification is performed below, and the simulation parameters are set as follows:

- (1) The number of data channels  $N$  of the TI-ADC cloud transmission platform is 4.
- (2) The sampling frequency of TI-ADC is  $\omega_s$ .
- (3) The number of quantization bits is 12 bit.
- (4) The frequency of the input sine signal is  $0.1001 \omega_s$ ;
- (5) The gain mismatch error of the data channel of each cloud transmission platform is Gain = [1, 1.1, 0.9, 1.02], and there is no other error.

It can be seen from Figure 4 that, in addition to the input signal component  $0.1001 \omega_s$  and its image component  $0.8999 \omega_s$ , there are also spurious components caused by gain mismatch at  $0.25 \pm 0.100 \omega_s$ ,  $0.5 \pm 0.1001 \omega_s$ , and  $0.75 \pm 0.1001 \omega_s$ . Its frequency is related to the frequency of the input signal. Due to the existence of gain error, the system SFDR is 25.24 dB, SNDR is 22.9893 dB, and ENOB is 3.5265 bit.

Delay mismatch is caused by the deviation between the actual sampling time and the ideal sampling time. There are many factors that cause delay deviation, which is mainly divided into two categories: deterministic delay deviation and random delay deviation. The deterministic delay deviation means that due to the mismatch of the front-end conditioning circuit, the difference between ADC chips, and the different length of the clock trace, the parameters of the data channels of the cloud transmission platform of the TI-ADC system are not completely consistent. This results in a fixed time difference between the actual sampling time and the ideal sampling time. The random delay deviation refers to the random delay difference caused by the jitter of the sampling clock and the different aperture delays of the data channels of different cloud transmission platforms. Clock jitter and aperture delay exist in any system, and we can regard them as Gaussian white noise. Therefore, we only consider the deterministic delay mismatch error, and the random delay deviation is not the focus of this study.

The HFB model of the delay mismatch error is shown in Figure 5.

In the figure,  $\tau_m$  is the delay error of the data channel of the  $m$ -th cloud transmission platform. From the figure, we can get the following:

$$x_m[n] = x[n + m - \tau_m]. \quad (16)$$

From equation  $Y(e^{j\omega T_s}) = \sum_{m=0}^{M-1} Y_m(e^{j\omega T_s}) = \frac{1}{M} \sum_{m=0}^{M-1} \sum_{k=0}^{M-1} X(e^{j(\omega T_s - 2\pi k/M)}) H_m(e^{j(\omega T_s - 2\pi k/M)})$

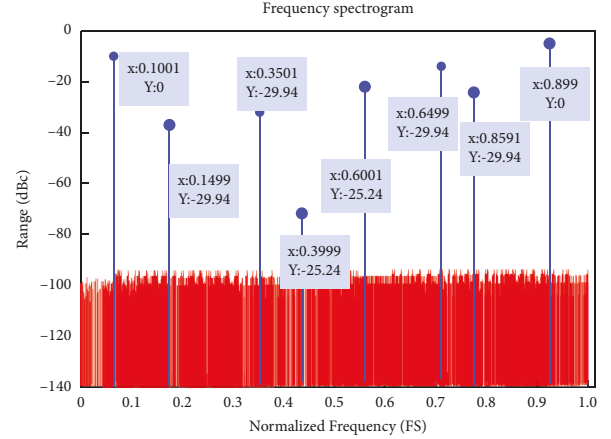


FIGURE 4: Gain mismatch spectrum.

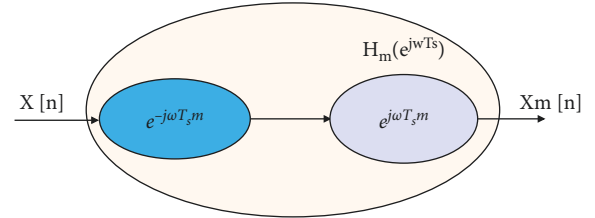


FIGURE 5: Delay mismatch HFB model.

$G_m(e^{j\omega T_s})$ , when there is a delay mismatch in the system, the output of TI-ADC is as follows:

$$Y(e^{j\omega T_s}) = \frac{1}{M} \sum_{m=0}^{M-1} \sum_{k=0}^{M-1} e^{-j2\pi km/M} e^{-j\omega T_s \tau_m} X(e^{j(\omega T_s - 2\pi k/N)}). \quad (17)$$

In order to find the influence of the delay mismatch error on the SNDR of the system, we also assume that the input signal is  $x(t) = \sin(2\pi f_c t)$  and the angular frequency is  $\omega_c$ . The data channel delay mismatch error  $\tau_m$  of the cloud transmission platform satisfies the Gaussian distribution, with a mean value of 0 and a variance of  $\sigma^2$ .

According to Parseval's theorem, the total power of the harmonics mismatched between the signal and the delay is as follows:

$$P_s + P_\tau = \frac{1}{2M} \sum_{m=0}^{M-1} |e^{-j\omega_c T_s \tau_m}|^2 = \frac{1}{2}. \quad (18)$$

The expansion of  $e^{-j\omega T_s \tau_m}$ 's Taylor series at 0 is as follows:

$$e^{-j\omega T_s \tau_m} \approx \sum_{p=0}^{\infty} \frac{(-j\omega T_s)^p}{p!} \tau_m^p. \quad (19)$$

Generally,  $\tau_m$  will be much less than one sampling period. We take the first three stages of the Taylor series as their value; then, the available signal power is [20] as follows:

$$P_s = \frac{1}{2} \left( 1 - \frac{1}{2} (\omega_c T_s)^2 \sigma^2 \right)^2. \quad (20)$$

Therefore, the power and SNDR of the mismatched harmonics can be obtained as follows:

$$P_\tau = \frac{1}{2}(\omega_c T_s)^2 \sigma^2, \quad (21)$$

$$\begin{aligned} \text{SNDR}_\tau &= 10 \log_{10} \frac{P_s}{P_\tau + N_q} \\ &= 10 \log_{10} \frac{1}{(\omega_c T_s)^2 \sigma^2 + 2N_q}. \end{aligned} \quad (22)$$

The simulation verification is performed below, and the simulation parameters are as follows:

- (1) The number of data channels  $N$  of the TI-ADC cloud transmission platform is 4.
- (2) The sampling frequency of TI-ADC is  $\omega_s$ .
- (3) The number of quantization bits is 12 bit.
- (4) The frequency of the input sine signal is  $0.1001 \omega_s$ .
- (5) The data channel delay mismatch error of each cloud transmission platform is Time = [0.05, -0.03, 0.1, 0.01], and there is no other error.

As shown in Figure 6, due to the delay error, the system SFDR is 19.38 dB, SNDR is 18.2946 dB, and ENOB is 2.7466 bit. It can be seen from the spectrogram that in addition to the input signal component  $0.1 \omega_s$  and its image component  $0.9 \omega_s$ , there are spurious components at  $0.25 \pm 0.1 \omega_s$ ,  $0.5 \pm 0.1 \omega_s$ , and  $0.75 \pm 0.1 \omega_s$  due to delay mismatch in the spectrum. The frequency of the spurious component is related to the input signal, and the position of the spurious component generated by the gain mismatch is the same.

The frequency-dependent mismatch is a gain mismatch and a delay mismatch with frequency-dependent characteristics, that is, each frequency point corresponds to different gain and delay mismatch parameters. The frequency-related mismatch error is caused by the ADC structure. We introduced the working principle of the ADC chip, and its hold function comes from the sample-and-hold. The structure diagram of the sample-and-hold device is shown in Figure 7(a).

The sample holder is composed of a holding switch, a switch buffer, an input signal buffer, an output signal buffer, and a strobe switch. The equivalent circuit of the sample-and-hold device is shown in Figure 7(b).

Among them,  $R$  represents the resistance of the strobe switch circuit, and  $C$  represents the equivalent sample-and-hold capacitance. The sample-and-hold device can be regarded as a filter, and its time constant is  $\tau = RC$ . Therefore, the expression of this first-order low-pass filter is as follows:

$$H_M(j2\pi f) = \frac{1}{1 + jf/f_{cm}} \quad m = 1, 2, \dots, M-1. \quad (23)$$

Among them,  $f_{cm} = 1/R_m C_m$  is the cut off frequency of the low-pass filter, and  $m$  is the data channel label of the cloud transmission platform. Due to process limitations, the switching circuit resistance and equivalent capacitance of

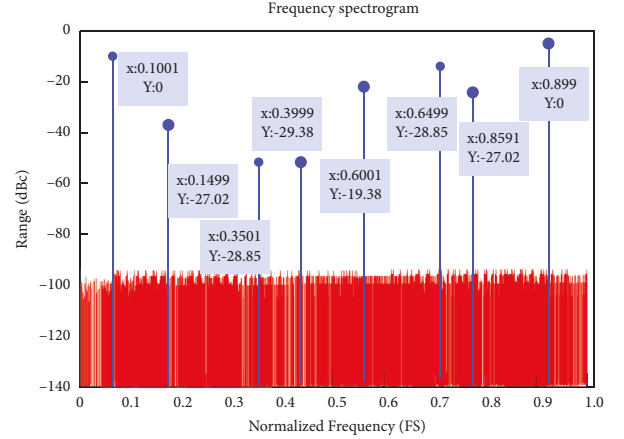


FIGURE 6: Time-delay mismatch spectrum diagram.

different ADCs cannot be completely the same. Therefore, the cloud transmission platform data channel response function of each cloud transmission platform data channel is also different, which is the source of frequency-related mismatch errors.

From the above analysis, it can be seen that the frequency-related mismatch error can be modeled as follows: each signal passes through a different low-pass filter, and the time constant error of the low-pass filter of each cloud transmission platform data channel is  $\Delta b_m = 1/f_{cm}$ . The frequency-dependent mismatch error can be equivalent to the combined error of the amplitude mismatch error and the phase mismatch error. The HFB model is shown in Figure 8 as follows:

Therefore, the input and output expressions of the cloud transmission platform data channel  $m$  are as follows:

$$x_m(n) = g_m(\omega)x(t + mT_s + \tau_m(\omega)) \quad m = 1, 2, \dots, M-1. \quad (24)$$

Among them,  $\omega$  represents the frequency of the input signal,  $g_m(\omega)$  represents the relationship function between the amplitude mismatch error and the signal frequency, and  $\tau_m(\omega)$  represents the relationship function between the phase mismatch error and the signal frequency.

The amplitude mismatch error here is different from the gain mismatch error discussed earlier. The difference is that the amplitude mismatch error is related to the frequency of the input signal. The phase mismatch error is also different from the delay mismatch error discussed earlier. The difference between them is that the phase mismatch error is nonlinearly related to the frequency of the input signal, while the delay mismatch error is linearly related to the frequency of the input signal.

From the formula  $Y(e^{j\omega T_s}) = \sum_{m=0}^{M-1} Y_m(e^{j\omega T_s}) = 1/M \sum_{k=0}^{M-1} X(e^{j(\omega T_s - 2\pi k/M)}) H_m(e^{j(\omega T_s - 2\pi k/M)}) G_m(e^{j\omega T_s})$ , when there is a frequency-related mismatch error, the output of the TI-ADC system is as follows:

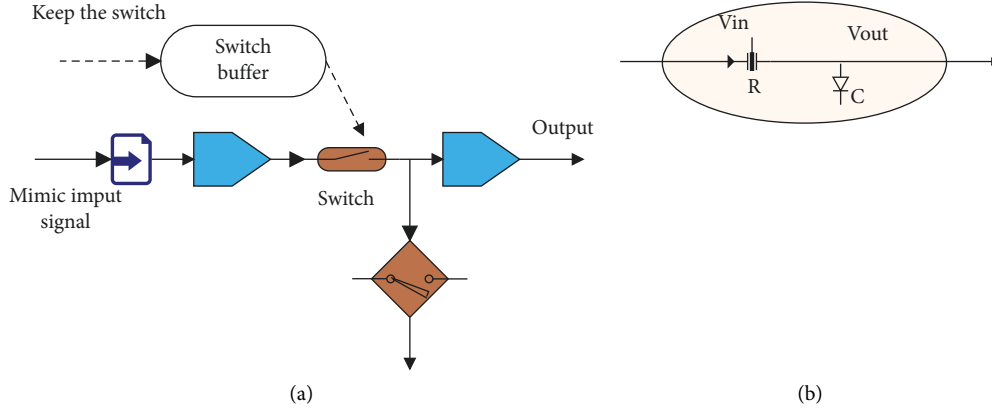


FIGURE 7: Diagram of sample holder. (a) Schematic diagram of sample-and-hold. (b) Sample-and-hold equivalent circuit diagram.

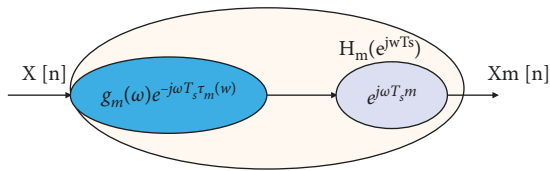


FIGURE 8: Frequency-dependent mismatch HFB model.

$$Y(e^{j\omega}) = \sum_{k=0}^{M-1} M(k) \cdot X(e^{j(\omega - 2\pi k/M)})$$

$$M(k) = \frac{1}{M} \sum_{m=0}^{M-1} e^{-j2\pi k/M m} g_m\left(\omega T_s - \frac{2\pi k}{M}\right) e^{j(\omega T_s - 2\pi k/M)\tau_m}.$$
(25)

Analyzing the above equation, when a single-frequency signal is an input to the system, the frequency-response mismatch spectrum has  $M-1$  mismatched harmonic components and mirrored components of the mismatched harmonics, which are the same as the spectrum of gain mismatch and delay mismatch. Since the frequency-dependent mismatch error is for wideband signals, it is impossible to formulate the effect of mismatch in the entire band. Therefore, we analyze a frequency point  $\omega_c$  in the passband and obtain the influence of frequency-dependent mismatch on system performance at this frequency point.

According to Parseval's theorem, the total power of the signal and mismatched harmonics is as follows:

$$P_s + P_q = \frac{1}{2} E[g_m^2(\omega_c)].$$
(26)

Using equation (21), the power of the signal is as follows:

$$P_s = \frac{1}{2} E[g_m^2(\omega_c)] \left(1 - \frac{1}{2} (\omega_c T_s)^2 \sigma_\tau(\omega_c)^2\right)^2.$$
(27)

For the sake of generality, we assume that the mean value of  $\tau_m(\omega_c)$  is 0, and the mean value of  $g_m(\omega_c)$  is 1. Then, at frequency  $\omega_c$ , the SNDR is as follows:

$$\text{SNDR}(\omega_c) = 10 \log_{10} \frac{P_s}{P_q + N_q}$$

$$= 10 \log_{10} \frac{1}{\sigma_g^2(\omega_c) + (\omega_c T_s)^2 \sigma_\tau(\omega_c) + 2N_q}.$$
(28)

Analysis of the above formula shows that, for a single-frequency point, the impact of frequency-dependent mismatch on the system is equal to the sum of the strengths of the amplitude mismatch and phase mismatch at this frequency point. Its spectrogram is similar to gain mismatch and delay mismatch, and will not be repeated here.

The delay mismatch error between the data channels of the cloud transmission platform is ultimately caused by the inconsistency of the sampling time between the data channels of the cloud transmission platform. Therefore, we can estimate the value at the ideal sampling point from the sampling sequence and use it to correct the delay deviation. This method is called time-domain interpolation, which is the most basic delay error compensation algorithm.

Interpolation is a very effective numerical processing method, and spline interpolation is one of the most commonly used methods. The cubic spline interpolation method is proposed to solve the second-order smoothness problem. The function fitted by this method consists of a piecewise cubic curve and has a continuous second-order derivative at the sampling point. When the system satisfies the over-sampling rate condition, the cubic spline interpolation method can be used to easily compensate for the system delay mismatch.

The definition of a cubic spline ULTRA function is as follows: the function is  $S(x) \in C^2[a, b]$ , which is a cubic polynomial on each partitioned interval  $[x_j, x_{j+1}]$ , and given  $n$  nodes  $x_1 < x_2 < x_3 < \dots < x_n$  in the interval, the function  $S(x)$  is a cubic spline function on nodes  $x_1, x_2, x_3, \dots, x_n$ . If a certain node  $x_j$  is given, its given function value is  $y_j = f(x_j)$ , and there are the following:

$$S(x_j) = y_j.$$
(29)

Then,  $S(x)$  is called the cubic spline value function. It can be seen from the above definition that if we want to obtain

$S(x)$ , we need to determine 4 parameters in each cell, and because there are  $n$  subintervals in the definition domain,  $4n$  parameters must be determined. According to the property that  $S(x)$  has a continuous second derivative in  $[a, b]$ , we can get the following:

$$\begin{aligned} S(x_j - 0) &= S(x_j + 0), S'(x_j - 0), \\ &= S'(x_j + 0), S''(x_j - 0), \\ &= S''(x_j + 0). \end{aligned} \quad (30)$$

That is,  $S(x)$  should satisfy the above continuity condition. When solving for the parameters,  $3(n-1)$  constraints can be obtained based on this condition, and together with  $S(x_j) = y_j$ , there are  $4n-2$  constraints. Therefore, 2 more constraints are needed to solve for the parameters.

Usually, boundary conditions can be added to the limit, the boundary conditions are given on two boundary points  $a$  and  $b$ , and generally, there are the following three types.

The value of the first derivative at the two ends is known, that is,

$$S'(x_0) = f'_0, S'(x_n) = f'_n. \quad (31)$$

The value of the second derivative at the two ends is known, that is,

$$S''(x_0) = f''_0, S''(x_n) = f''_n. \quad (32)$$

There is a special case  $S''(x_0) = S''(x_n) = 0$ , which is called a natural boundary condition.

If  $f(x)$  is a periodic function with  $x_n - x_0$  as the period, it should satisfy the following:

$$\begin{aligned} S(x_0 + 0) &= S(x_n - 0), S'(x_0 + 0), \\ &= S'(x_n - 0), \\ S''(x_0 + 0) &= S''(x_n - 0). \end{aligned} \quad (33)$$

From equation (29) and boundary conditions, the following function is constructed as follows:

$$S(x) = \sum_{j=0}^n [y_j \alpha_j(x) + m_j \beta(j)]. \quad (34)$$

Among them,  $\alpha_j(x)$  and  $\beta(j)$  are the value basis functions of the third-order Hermite value polynomial,  $m_j = S'(x_j)$ . In the interval  $[x_j, x_{j+1}]$ ,  $S''(x)$  can be expressed as follows:

$$S'(x) = M_j \frac{x_{j+1} - x}{h_j} + M_{j+1} \frac{x - x_j}{h_j}. \quad (35)$$

Among them,  $M_j = S''(X_j, h_j = x_{j+1} - x_j)$ , performs two integral operations on  $S''(x)$ , and according to the conditions  $S(x_j) = y_j, S(x_{j+1}) = y_{j+1}$ , the expression of cubic spline function  $S(x)$  can be obtained, as shown below as follows:

$$\begin{aligned} S(x) &= M_j \frac{(x_{j+1} - x)^3}{6h_j} + M_{j+1} \frac{(x - x_j)^3}{6h_j} + \left( y_j - \frac{M_j h_j^2}{6} \right) \frac{x_{j+1} - x}{h_j} \\ &\quad - \frac{M_{j+1} - M_j}{6} h_j. \end{aligned} \quad (36)$$

From equation (36), we can get the following:

$$S'(x_j + 0) = -\frac{h_j}{3} M_j - \frac{h_j}{6} M_{j+1} + \frac{y_{j+1} - y_j}{h_j}, \quad (37)$$

$$S'(x_j - 0) = -\frac{h_{j-1}}{6} M_{j-1} - \frac{h_{j-1}}{3} M_j + \frac{y_j - y_{j-1}}{h_{j-1}}.$$

Furthermore, according to  $S'(x_j + 0) = S'(x_j - 0)$ , the above formula can be combined to obtain the following:

$$u_j M_{j-1} + 2M_j + \lambda_j M_{j+1} = d_j. \quad (38)$$

Among them,  $u_j = h_{j-1}/h_{j-1} + h_j, \lambda_j = h_j/h_{j-1} + h_j, d_j = 6f[x_j, x_{j+1}] - f[x_{j-1}, x_j]/h_{j-1} + h_j, f[x_j, x_{j+1}] = y_{j+1} - y_j/h_j$ , and then considering the boundary conditions, we can get the following:

$$M_0 = M_n, u_n M_{n-1} + 2M_n + \lambda_n M_{n+1} = d_n. \quad (39)$$

Among them,  $\lambda_n = h_0/h_{n-1} + h_0, u_n = 1 - \lambda_n = h_{n-1}/h_{n-1} + h_0, d_n = 6f[x_0, x_1] - f[x_{n-1}, x_n]/h_{n-1} + h_0$ . In summary, the matrix can be obtained, as shown below as follows:

$$\begin{bmatrix} 2 & \lambda_1 & & & u_1 \\ u_2 & 2 & \lambda_2 & & \\ & \ddots & \ddots & \ddots & \\ & & u_{n-1} & 2 & \lambda_{n-1} \\ \lambda_n & & & u_n & 2 \end{bmatrix} \begin{bmatrix} M_1 \\ M_2 \\ \vdots \\ M_{n-1} \\ M_n \end{bmatrix} = \begin{bmatrix} d_1 \\ d_2 \\ \vdots \\ d_{n-1} \\ d_n \end{bmatrix}. \quad (40)$$

According to this matrix,  $M_j$  can be obtained, and then, the cubic spline value function  $S(x)$  can be obtained.

The simulation process is as follows.

Taking the data channel TI-ADC of the two cloud transmission platform as an example, the system sampling period is  $T_s$  and the sampling rate is  $\omega_s$ . The signal to be sampled is sinusoidal, and the mismatched signal is compensated by interpolation, and the result is shown in Figure 9.

It can be seen from the test results that when the signal frequency is relatively low relative to the sampling frequency, the spline interpolation algorithm can well compensate for the signal mismatch. As the frequency of the input signal increases, the system cannot meet its oversampling requirements, and the



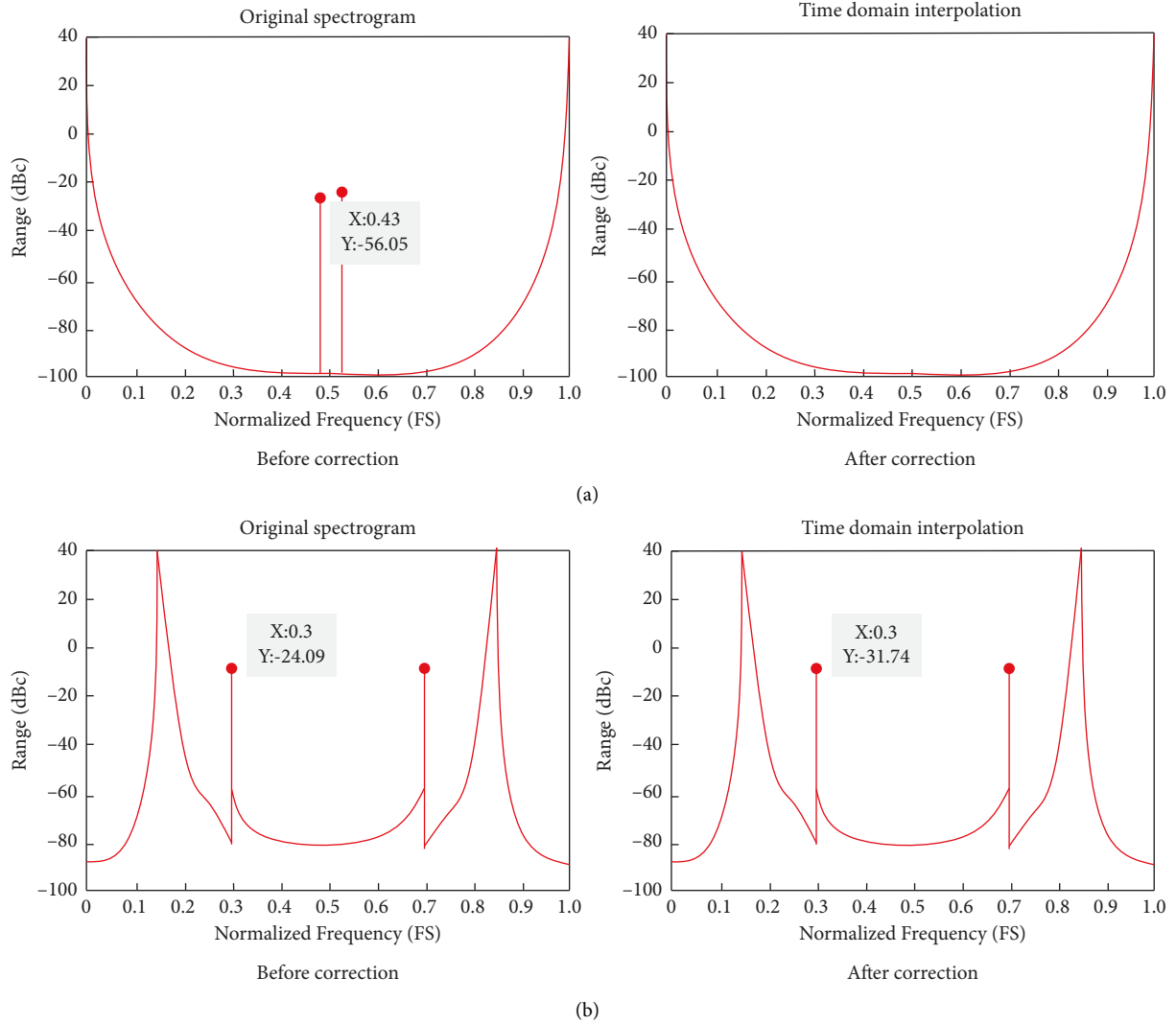


FIGURE 9: Interpolation method to compensate the test results of mismatched signals. (a) The input signal frequency is  $0.01 \omega_s$ . (b) The input signal frequency is  $0.2 \omega_s$ .

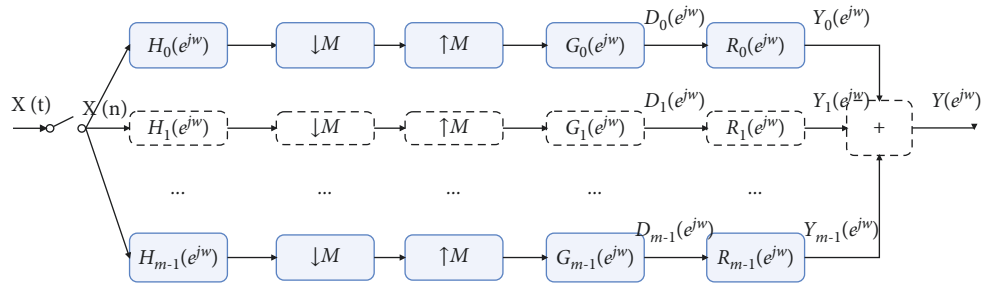


FIGURE 10: Perfect reconstruction filter model.

compensation effect is greatly reduced at this time. Therefore, when oversampling is satisfied, the interpolation method can be used for mismatch compensation.

The perfect reconstruction filter bank is based on the HFB model, adding a correction filter to each subpath, so that the combined signal after correction is consistent with

the original signal, and its structure diagram is shown in Figure 10. The following derives the reconstruction conditions of the perfect reconstruction filter.

For channel  $m$ , the output signal  $D_m(e^{j\omega T_s})$  with delay mismatch error or frequency-dependent mismatch error is as follows:

$$D_m(e^{j\omega T_s}) = \frac{1}{M} \sum_{k=0}^{M-1} X(e^{j(\omega T_s - 2\pi k/M)}) e^{-j2\pi k/Mm} g_m\left(\omega T_s - \frac{2\pi k}{M}\right) e^{j(\omega T_s - 2\pi k/M)\tau_m}. \quad (41)$$

In the formula,  $g_m$  is the gain mismatch function of the data channel of the  $m$  cloud transmission platform,  $\tau_m$  is the delay mismatch function (in  $T_s$  as the unit, normalized

value), and the output of the mismatch signal after passing the correction filter is as follows:

$$Y_m(e^{j\omega T_s}) = \frac{1}{M} \sum_{k=0}^{M-1} X(e^{j(\omega T_s - 2\pi k/M)}) e^{-j2\pi k/Mm} g_m\left(\omega T_s - \frac{2\pi k}{M}\right) e^{j(\omega T_s - 2\pi k/M)\tau_m} R_m(e^{j\omega T_s}). \quad (42)$$

In the formula,  $R_m(e^{j\omega T_s})$  is the correction filter function of the cloud transmission platform data channel  $m$ .

Thus, the combined output can be obtained as follows:

$$Y(e^{j\omega T_s}) = \frac{1}{M} \sum_{m=0}^{M-1} \sum_{k=0}^{M-1} X(e^{j(\omega T_s - 2\pi k/M)}) e^{-j2\pi k/Mm} g_m\left(\omega T_s - \frac{2\pi k}{M}\right) e^{j(\omega T_s - 2\pi k/M)\tau_m} R_m(e^{j\omega T_s}). \quad (43)$$

We set up the following:

$$M(k) = \frac{1}{M} \sum_{m=0}^{M-1} e^{-j2\pi k/Mm} g_m\left(\omega T_s - \frac{2\pi k}{M}\right) e^{j(\omega T_s - 2\pi k/M)\tau_m} R_m(e^{j\omega T_s}). \quad (44)$$

The combined output is as follows:

$$Y(e^{j\omega T_s}) = \sum_{k=0}^{M-1} X(e^{j(\omega T_s - 2\pi k/M)}) M(k). \quad (45)$$

It can be seen from the above formula that if you want the output of the system to be error-free, the output should only contain the spectral components of the input signal, and then,  $M(k)$  should meet the following conditions:

$$M(k) = \begin{cases} c e^{-j\omega d} & k = 0, \\ 0 & \text{other.} \end{cases} \quad (46)$$

Among them,  $c$  is a constant and  $d$  is a definite time delay, which is the condition for perfect reconstruction. Therefore, by solving the correction filter  $R_m$  according to the perfect reconstruction condition, the error compensation can be realized.

From the perfect reconstruction condition and equation (44), the following matrix expression can be obtained as follows:

$$M = H \times R. \quad (47)$$

Among them, there are the following:

$$H = \frac{1}{M}$$

$$\begin{aligned} [M = [ & c \cdot e^{-j\omega d} \cdot 0 \cdots 0 e^{-j2\pi 0/M} H_0(\omega) e^{-j2\pi 0/M_1} H_1(\omega) \cdot e^{-j2\pi 0/M(M-1)} H_{M-1}(\omega) e^{-j2\pi 1/M} H_0(\omega) e^{-j2\pi 1/M_1} H_1(\omega) \cdot e^{-j2\pi 1/M(M-1)} H_{M-1}(\omega) \\ & \vdots \vdots \vdots e^{-j2\pi(M-1)/M} H_0(\omega) e^{-j2\pi(M-1)/M_1} H_1(\omega) \cdot e^{-j2\pi(M-1)/M(M-1)} H_{M-1}(\omega) ]. \end{aligned} \quad (48)$$

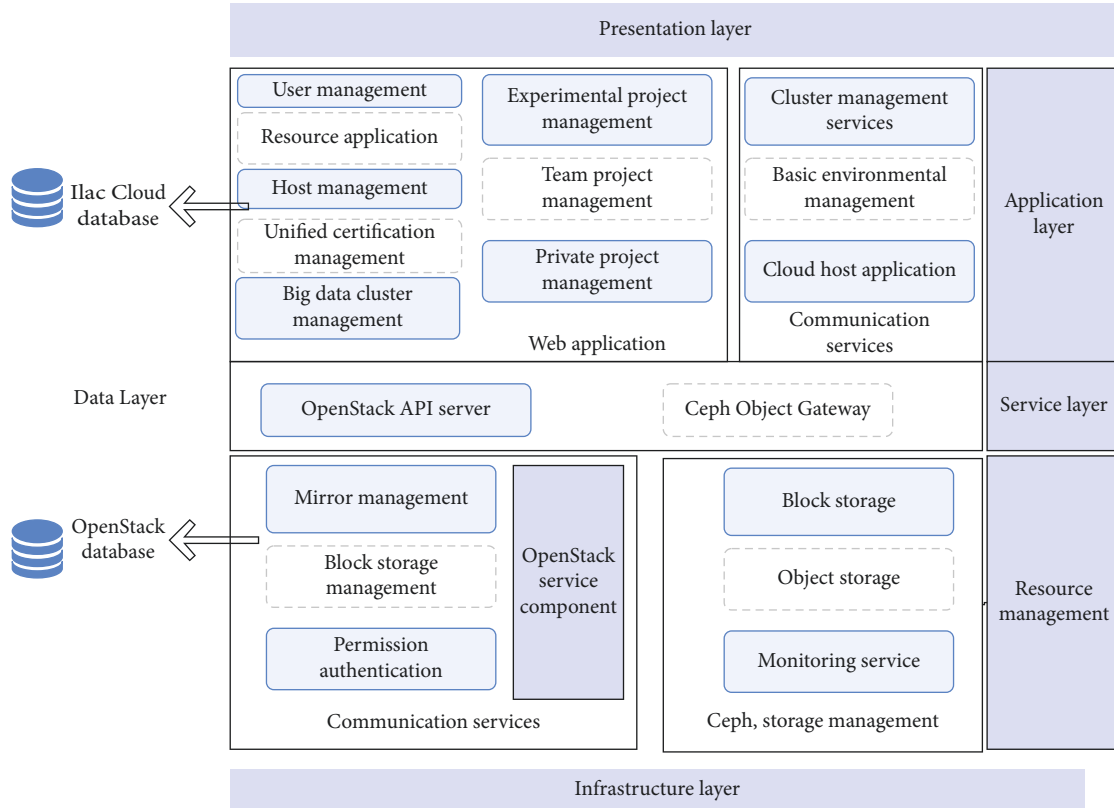


FIGURE 11: The overall architecture of the college Japanese intensive reading teaching system based on the network cloud platform.

$H$  is a matrix composed of the cloud transmission platform data channel mismatch function  $H_m$ , and  $R$  is a matrix composed of the correction filter  $R_m$  of each cloud transmission platform data channel. From this, the frequency-response function of the correction filter can be obtained, that is,

$$R = H^{-1} \times M. \tag{49}$$

In summary, the process of using the perfect reconstruction filter algorithm to compensate for the frequency-dependent mismatch error of the broadband signal is as follows:

- (1) This study selects  $N$  frequency points ( $0 \sim N - 1$ ) in the passband range and uses the error mismatch estimation algorithm to estimate the gain mismatch error and delay mismatch error of each channel. Subsequently, the error value at each discrete point is fitted to obtain the data channel mismatch function  $H_m(\omega)$  of each cloud transmission platform.
- (2) In this study, these  $N$  frequency points are substituted into equation (49) in turn, and  $N$  equations can be obtained. Each equation can obtain the response value of the corresponding frequency point of the correction filter  $R_m$ .
- (3) This study performs IFFT operation on  $R_m$  to obtain filter coefficients.

- (4) The data channel mismatch signal of each cloud transmission platform is convolved with the corresponding correction filter.
- (5) This study adds the corrected signals of each channel to obtain the reconstructed signal.

#### 4. The Teaching Mode of Japanese Intensive Reading Colleges and Universities Based on the Network Cloud Platform

The overall architecture of the college Japanese intensive reading teaching system based on the network cloud platform includes the following layers: application layer, service layer, resource management layer, infrastructure layer, and data layer for intensive reading teaching. The hierarchical thinking can make the entire system structure clearer and easier to expand and maintain. The overall architecture diagram is shown in Figure 11.

The overall functional module design of the system is shown in Figure 12.

Through the above analysis, a college Japanese intensive reading teaching system based on the network cloud platform has been constructed. This study counts multiple sets of data to evaluate the teaching effect of the college Japanese intensive reading teaching system based on the network cloud platform proposed in this study. Moreover, this study combines simulation research and expert evaluation to

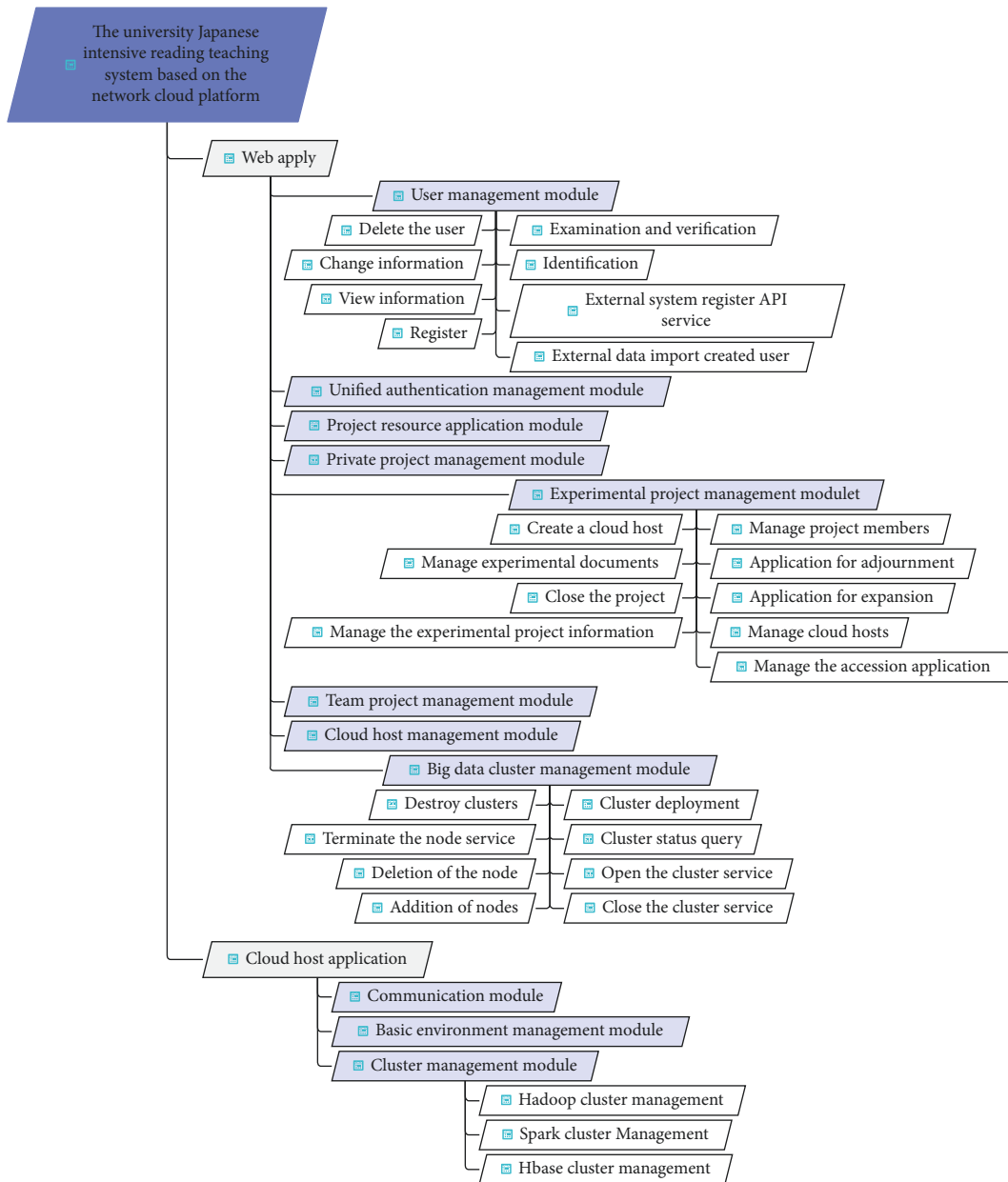


FIGURE 12: Functional modules of college Japanese intensive reading teaching system based on the network cloud platform.

evaluate the resource processing and teaching effect of this system, and the results shown in Tables 1 and 2 are obtained. The corresponding statistical graphs are shown in Figures 13 and 14.

Through the above research, it can be known that the college Japanese intensive reading teaching system based on the network cloud platform has a good resource processing effect and teaching effect of Japanese intensive reading teaching.

TABLE 1: Teaching resource processing effect of college Japanese intensive reading teaching system based on the network cloud platform.

Number	Cloud resource processing	Number	Cloud resource processing
1	95.97	25	96.15
2	96.13	26	96.37
3	97.07	27	95.24
4	97.14	28	96.03
5	96.91	29	95.58
6	97.71	30	97.45
7	95.64	31	95.65
8	97.28	32	94.69
9	93.16	33	94.34
10	94.93	34	97.39
11	93.14	35	95.18
12	95.52	36	96.36
13	94.52	37	93.52
14	93.84	38	97.65
15	97.56	39	94.47
16	94.87	40	95.85
17	94.41	41	97.04
18	93.15	42	93.54
19	96.78	43	97.45
20	96.85	44	94.20
21	94.92	45	94.89
22	97.61	46	95.90
23	94.73	47	97.17
24	94.69		

TABLE 2: Teaching effect of college Japanese intensive reading teaching system based on the network cloud platform.

Number	Teaching effect	Number	Teaching effect
1	78.45	25	78.89
2	89.78	26	79.48
3	85.78	27	82.97
4	86.44	28	91.37
5	90.47	29	87.04
6	91.54	30	90.84
7	79.79	31	87.84
8	82.01	32	86.38
9	91.61	33	89.56
10	80.12	34	77.62
11	88.34	35	79.84
12	80.05	36	78.31
13	88.12	37	83.68
14	80.96	38	87.73
15	79.73	39	84.26
16	85.92	40	90.55
17	88.53	41	80.17
18	78.29	42	83.30
19	77.38	43	88.75
20	82.88	44	81.31
21	90.23	45	85.62
22	81.01	46	83.27
23	84.11	47	90.49
24	88.12		

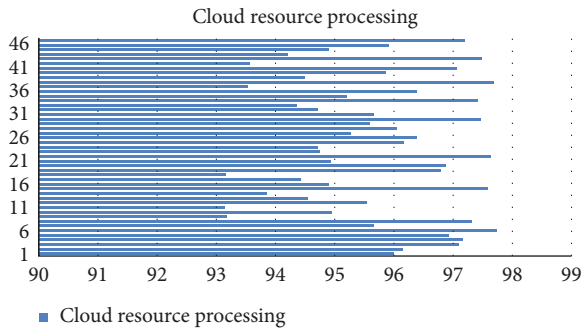


FIGURE 13: Teaching resource processing effect of college Japanese intensive reading teaching system.

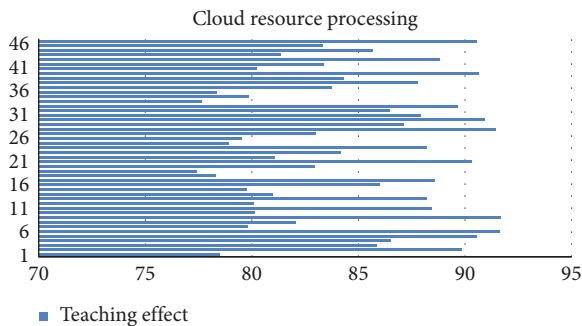


FIGURE 14: Teaching effect of college Japanese intensive reading teaching system based on the network cloud platform.

## 5. Conclusion

The main purpose of Japanese teaching in colleges and universities is to cultivate skilled, applied, practical, and compound senior foreign language talents who meet the needs of the social market, have strong Japanese language application ability, can use Japanese as a tool, and engage in relevant professional practice activities. Therefore, Japanese teaching in colleges and universities should focus on cultivating students' language application and practical ability. As one of the compulsory courses for Japanese majors, the Japanese intensive reading course is a comprehensive course that cultivates students' listening, speaking, reading, writing, and translation skills. College students have poor self-learning ability and short school time. Therefore, how to effectively use Japanese intensive reading courses to improve students' comprehensive practical ability in Japanese is a question that every Japanese teacher must think about. In order to improve the teaching effect of Japanese intensive reading in colleges and universities, this study combines the network cloud platform to improve Japanese intensive reading teaching in colleges and universities, and builds an intelligent Japanese intensive reading teaching system. The research shows that the college Japanese intensive reading teaching system based on the network cloud platform has a good resource processing effect and teaching effect of Japanese intensive reading teaching.

## Data Availability

The labeled datasets used to support the findings of this study are available from the corresponding author upon request.

## Conflicts of Interest

The authors declare that they have no conflicts of interest.

## Acknowledgments

This study was sponsored by the Key Teaching Study Project of 2020 College and University Quality Program in Anhui Province (project no. 2020jyxm0730).

## References

- [1] S. F. M. Alfalah, "Perceptions toward adopting virtual reality as a teaching aid in information technology," *Education and Information Technologies*, vol. 23, no. 6, pp. 2633–2653, 2018.
- [2] G. Cooper, H. Park, Z. Nasr, L. P. Thong, and R. Johnson, "Using virtual reality in the classroom: preservice teachers' perceptions of its use as a teaching and learning tool," *Educational Media International*, vol. 56, no. 1, pp. 1–13, 2019.
- [3] J. Zhao, X. Xu, H. Jiang, and Y. Ding, "The effectiveness of virtual reality-based technology on anatomy teaching: a meta-analysis of randomized controlled studies," *BMC Medical Education*, vol. 20, no. 1, pp. 127–139, 2020.
- [4] S. J. Bennie, K. E. Ranaghan, H. Deeks et al., "Teaching enzyme catalysis using interactive molecular dynamics in virtual reality," *Journal of Chemical Education*, vol. 96, no. 11, pp. 2488–2496, 2019.
- [5] S. F. M. Alfalah, J. F. M. Falah, T. Alfalah, M. Elfalah, N. Muhaidat, and O. Falah, "A comparative study between a virtual reality heart anatomy system and traditional medical teaching modalities," *Virtual Reality*, vol. 23, no. 3, pp. 229–234, 2019.
- [6] V. L. Dayarathna, S. Karam, R. Jaradat et al., "Assessment of the efficacy and effectiveness of virtual reality teaching module: a gender-based comparison," *International Journal of Engineering Education*, vol. 36, no. 6, pp. 1938–1955, 2020.
- [7] O. Hernandez-Pozas and H. Carreon-Flores, "Teaching international business using virtual reality," *Journal of Teaching in International Business*, vol. 30, no. 2, pp. 196–212, 2019.
- [8] V. Andrunyk, T. Shestakevych, and V. Pasichnyk, "The technology of augmented and virtual reality in teaching children with ASD," *Econtechmod: Scientific Journal*, vol. 7, no. 4, pp. 59–64, 2018.
- [9] R. Mayne and H. Green, "Virtual reality for teaching and learning in crime scene investigation," *Science & Justice*, vol. 60, no. 5, pp. 466–472, 2020.
- [10] M. Taubert, L. Webber, T. Hamilton, M. Carr, and M. Harvey, "Virtual reality videos used in undergraduate palliative and oncology medical teaching: results of a pilot study," *BMJ Supportive & Palliative Care*, vol. 9, no. 3, pp. 281–285, 2019.
- [11] K. E. McCool, S. A. Bissett, T. L. Hill, L. A. Degernes, and E. C. Hawkins, "Evaluation of a human virtual-reality endoscopy trainer for teaching early endoscopy skills to veterinarians," *Journal of Veterinary Medical Education*, vol. 47, no. 1, pp. 106–116, 2020.
- [12] X. Xu, P. Guo, J. Zhai, and X. Zeng, "Robotic kinematics teaching system with virtual reality, remote control and an on-site laboratory," *International Journal of Mechanical Engineering Education*, vol. 48, no. 3, pp. 197–220, 2020.
- [13] P. W. Chang, B. C. Chen, C. E. Jones, K. Bunting, C. Chakraborti, and M. J. Kahn, "Virtual reality supplemental teaching at low-cost (VRSTL) as a medical education adjunct for increasing early patient exposure," *Medical Science Educator*, vol. 28, no. 1, pp. 3–4, 2018.

- [14] J. Zhang and Y. Zhou, "Study on interactive teaching laboratory based on virtual reality," *International Journal of Continuing Engineering Education and Life Long Learning*, vol. 30, no. 3, pp. 313–326, 2020.
- [15] R. Ramlogan, A. U. Niazi, R. Jin, J. Johnson, V. W. Chan, and A. Perlas, "A virtual reality simulation model of spinal ultrasound: role in teaching spinal sonoanatomy," *Regional Anesthesia and Pain Medicine*, vol. 42, no. 2, pp. 217–222, 2017.
- [16] Y. C. Hsu, "Exploring the learning motivation and effectiveness of applying virtual reality to high school mathematics," *Universal Journal of Educational Research*, vol. 8, no. 2, pp. 438–444, 2020.
- [17] J. D. Anacona, E. E. Millán, and C. A. Gómez, "Aplicación de los metaversos y la realidad virtual en la enseñanza," *Entre Ciencia e Ingeniería*, vol. 13, no. 25, pp. 59–67, 2019.
- [18] P. Calvert, "Virtual reality as a tool for teaching library design," *Education for Information*, vol. 35, no. 4, pp. 439–450, 2019.
- [19] J. Morimoto and F. Ponton, "Virtual reality in biology: could we become virtual naturalists?" *Evolution: Education and Outreach*, vol. 14, no. 1, pp. 7–13, 2021.
- [20] D. Checa and A. Bustillo, "Advantages and limits of virtual reality in learning processes: briviesca in the fifteenth century," *Virtual Reality*, vol. 24, no. 1, pp. 151–161, 2020.